Joint 3D Positioning and Network Synchronization in 5G Ultra-Dense Networks Using UKF and EKF

Mike Koivisto*, Mário Costa†, Aki Hakkarainen*, Kari Leppänen†, and Mikko Valkama*
* Department of Electronics and Communications Engineering, Tampere University of Technology, Finland
Emails: {mike.koivisto, aki.hakkarainen, mikko.e.valkama}@tut.fi
† Huawei Technologies Oy (Finland) Co., Ltd, Finland R&D Center
Emails: {mariocosta, kari.leppanen}@huawei.com

***Abstract*—It is commonly expected that future fifth generation (5G) networks will be deployed with a high spatial density of access nodes (ANs) in order to meet the envisioned capacity requirements of the upcoming wireless networks. Densification is beneficial not only for communications but it also creates a convenient infrastructure for highly accurate user node (UN) positioning. Despite the fact that positioning will play an important role in future networks, thus enabling a huge amount of location-based applications and services, this great opportunity has not been widely explored in the existing literature. Therefore, this paper proposes an unscented Kalman filter (UKF)-based method for estimating directions of arrival (DoAs) and times of arrival (ToA) at ANs as well as performing joint 3D positioning and network synchronization in a network-centric manner. In addition to the proposed UKF-based solution, a similar extended Kalman filter (EKF)-based method is proposed by extending the existing 2D EKF-based approach to cover also realistic 3D scenarios. Building on the premises of 5G ultra-dense networks (UDNs), the performance of both methods is evaluated and analysed in terms of DoA and ToA estimation as well as positioning and clock offset estimation accuracy, using the METIS map-based ray-tracing channel model and 3D trajectories for vehicles and unmanned aerial vehicles (UAVs) through the Madrid grid. Based on the comprehensive numerical evaluations, both proposed methods can provide the envisioned one meter 3D positioning accuracy even in the case of unsynchronized 5G network while simultaneously tracking the clock offsets of network elements with a nanosecond-scale accuracy.**

***Index Terms*—3D, 5G networks, Positioning, Synchronization, Unscented Kalman Filter**

I. Introduction

In contrast to earlier generations, the structure of future fifth generation (5G) networks will change dramatically in order to meet the envisioned requirements in terms of, e.g., high data rates and latency. To achieve these demanding requirements, it is commonly expected that 5G networks will be deployed with wideband waveforms at high, even above 6 GHz frequencies due to better spectrum availability [1]–[3]. Furthermore, it is envisioned that spatial density of access nodes (ANs) will simultaneously increase resulting in so-called ultra-dense networks (UDNs) [3]–[5]. Thus, user nodes (UNs) will be most likely within the range of several ANs leading to a scenario where devices will also be in a line-of-sight (LoS) condition with a few ANs most of the time [6], [7]. Such a condition is beneficial not only for communication purposes but it also creates a great opportunity for device positioning based on highly accurate time of arrival (ToA) estimates that can be obtained at LoS-ANs due to the envisioned wideband waveforms. In addition, ANs in 5G are expected to be equipped with smart antenna solutions, such as antenna arrays, enabling also estimation of directions of arrival (DoAs). This directional information can be, in turn, fused with ToA estimates to achieve improved positioning performance.

Technically, positioning in 5G networks can be carried out either within devices or in a network-centric manner, where the central unit of a network tracks the devices within the network. However, the latter option has several advantages over the device-centric approach. First, network-centric positioning is more energy efficient from the devices' perspective since the actual computational effort is done in the central units of networks, thus saving the batteries of UNs. Furthermore, uplink (UL) pilot signals, which are anyway exchanged between the UNs and ANs for channel estimation and scheduling on time division duplex (TDD) networks [8], can be utilized for highly accurate positioning without the need of allocating specific reference signals for positioning [9]. This means, in turn, that such positioning engine can be continuously running in the background providing up-to-date location information for necessary systems and applications with a low latency.

In general, 5G has a great potential to achieve the envisioned positioning accuracy of one meter or even less [3], consequently outperforming existing positioning techniques such as global positioning system (GPS) and wireless local area network (WLAN) fingerprinting based methods, in which the positioning accuracy is usually in the order of couple of meters [10]. Such a significant improvement in positioning accuracy creates an opportunity for huge amount of future location-based applications, e.g., intelligent traffic systems (ITSs), autonomous vehicles, and proactive radio resource management (RRM) [11]. Despite the fact that positioning will naturally play an important role in future 5G networks, the potential for positioning in such networks has not been widely recognized in the existing literature.

In the past, the extended Kalman filters (EKFs) have been proposed for 2D target tracking using DoA measurements only [12], but also a combination of DoA and ToA measurements is used for tracking devices in a synchronized network [13]. In addition, the authors in [9] proposed a method for joint device positioning

This work was supported by the Finnish Funding Agency for Technology and Innovation (Tekes), under the projects "5G Networks and Device Positioning", "TAKE-5", and "Future Small-Cell Networks using Reconfigurable Antennas".

Online videos available at `http://www.tut.fi/5G/GLOBECOM16`

and synchronization using DoAs and ToAs in future 5G networks in order to relax a synchronization assumption. Furthermore, realism was increased in [14] by assuming not only an unsynchronized UN but also unsynchronized ANs in an EKF-based joint 2D positioning and network synchronization method. In [15], non-sequential estimation methods for simultaneous 2D positioning and network synchronization were proposed assuming a static network with known AN clock parameters. In contrast to the proposed 2D positioning solutions, in [16] a joint DoA and ToA based method also for 3D device location estimation using only one AN in a synchronized network was proposed. However, the authors in [16] did not propose any iterative filtering method to obtain continuous position estimates for the devices.

In this paper, an unscented Kalman filter (UKF)-based cascaded solution for the joint DoA and ToA estimation, and simultaneous 3D device positioning and network synchronization in future 5G UDNs is proposed. In the first phase of the proposed cascaded solution, a UKF-based estimation and tracking method for both DoAs and ToAs, which stems from [14], is performed. Thereafter, the obtained estimates are fused within the joint 3D device positioning and network synchronization UKF, later referred to as the joint DoA/ToA Pos&Clock UKF or joint DoA/ToA Pos&Sync UKF depending on whether the ANs composing the network are assumed to be synchronized among each other or phase-locked, respectively. As a result, the proposed method provides not only 3D position estimates for a UN but also clock offset estimates for the UN and LoS-ANs. In addition to the UKF-based approach, a similar 3D EKF-based solution is proposed for the comparison purposes by extending the existing 2D EKF-based method [14] to cover also realistic 3D scenarios. In contrast to earlier studies, the proposed methods provide highly accurate and sequential 3D position estimates for the UNs, thus enabling tracking of unmanned aerial vehicles (UAVs), for example.

The rest of the paper is organized as follows. In Section II, necessary assumptions about the network, used positioning engine as well as channel model are discussed. Thereafter, a general algorithm for the UKF is presented in Section III, and more detailed models for the UKF- and EKF-based DoA and ToA estimation, as well as simultaneous UN positioning and network synchronization are presented in Sections IV and V, respectively. In Section VI, the employed simulation environment is explained together with the assumptions made before the actual numerical results and analysis of the proposed method are presented. Finally, conclusions are drawn in Section VII.

II. System Model

A. 5G Network and Positioning Engine

In this paper, following the key 5G white papers [3]–[5], an outdoor network with densely deployed ANs is considered as illustrated in Fig. 1. In the assumed network, the ANs are attached to lamp posts $7\,\mathrm{m}$ above the ground and with an inter-site distance (ISD) of around $50\,\mathrm{m}$ or even less as illustrated in [14]. The deployed ANs are also assumed to be equipped with antenna arrays which enable DoA estimation at ANs. In the considered network, the ANs consist of cylindrical antenna arrays in which 10 dual-polarized cross-dipoles are placed along

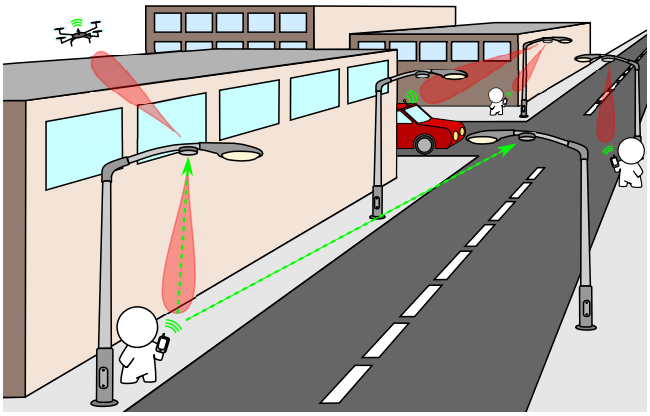

Fig. 1. Densely deployed ANs attached to lamp posts in an outdoor UDN with several connected devices. In the proposed method, UN positioning and network synchronization are performed in a network-centric manner in order to reduce energy consumption of the devices.

two circles. However, other multiantenna solutions can be used as well. For the sake of simplicity, the locations of ANs, denoted as $\mathbf{p}_{\ell_i} = [x_{\ell_i}, y_{\ell_i}, z_{\ell_i}]^{\mathrm{T}}$ where ℓ_i denotes the index of an AN, are assumed to be known using, e.g., information from GPS.

In the considered network, UNs periodically transmit UL pilot signals which will be later referred to as beacons. The beacons are assumed to employ an orthogonal frequency-division multiplexing (OFDM) waveform, in the form of orthogonal frequency-division multiple access (OFDMA) in a multiuser network. The beacons are used to obtain channel state information (CSI) at ANs [8] but these beacons can be also utilized for network-centric positioning, thus leading to an "always-on" positioning solution. It is assumed that the ANs will detect whether or not they are in LoS condition with a UN based on the received beacons. Such a LoS condition can be determined using, e.g., the Rice factor of the received signal strength (RSS) [17], which is typically 10-$20\,\mathrm{dB}$ in UDNs [7]. Each LoS-AN will then estimate DoAs and ToAs using the received beacons within the DoA/ToA UKFs or EKFs, and these estimates are thereafter gathered from all LoS-ANs and fused into a 3D UN position estimate in the central entity of the network using either the proposed UKF- or EKF-based joint DoA/ToA Pos&Clock or Pos&Sync estimation methods as depicted in Fig. 2.

B. Clock Models

In general, the clocks within devices are equipped with relatively cheap oscillators which, in turn, leads to time-varying clock offsets in such devices. Due to these imperfections, a progressive model is required in order to characterize or estimate clock offsets of the devices. It is shown in [18] that clock offset ρ for two consecutive time instants $k-1$ and k are related such that

$$\rho[k] = \rho[k-1] + \alpha[k]\Delta t, \tag{1}$$

where Δt is the time period between the instants $k-1$ and k, and $\alpha[k]$ denotes the clock skew which is a time-varying quantity as well. Based on observations, e.g., in [18], the average clock skew can be considered constant but in this paper, the following time-dependent clock skew model that stems from [18]

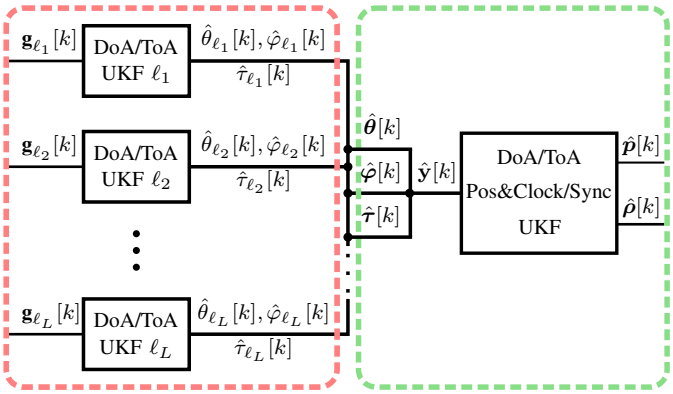

Fig. 2. In the DoA and ToA estimation phase (red color), channel estimates $\mathbf{g}$ are used within the DoA/ToA UKFs at each LoS-AN to obtain azimuth and elevation angle as well as ToA estimates denoted as $\hat{\varphi}$ and $\hat{\theta}$, and $\hat{\tau}$, respectively. The estimates are then fused within the joint DoA/ToA Pos&Clock/Sync UKF into a UN position estimate $\hat{\mathbf{p}}$ and clock offset estimates $\hat{\boldsymbol{\rho}}$ in the second phase of the proposed solution (green color). The proposed 3D EKF-based solutions can be represented by replacing the UKFs with the EKFs.

and encompasses also the constant clock skew model as a special case is considered

$$\alpha[k] = \zeta\alpha[k-1] + \eta[k], \tag{2}$$

where $\eta[k] \sim \mathcal{N}(0, \sigma_\eta^2)$ is an additive Gaussian white-noise sequence and ζ is a constant model parameter such that $|\zeta| \leq 1$.

Two different scenarios for synchronization within a network are considered. In the first scenario, UNs have unsynchronized clocks where only the necessary timing and frequency synchronization to avoid inter-carrier-interference (ICI) and inter-symbol-interference (ISI) is assumed. On the other hand, ANs in such a scenario are assumed to have synchronized clocks among each other. In the second and more realistic scenario, clocks within ANs are phase-locked, i.e., the unknown clock offsets of ANs are not fundamentally varying over the real time, whereas clocks within UNs are assumed to be unsynchronized. The aforementioned synchronized and phase-locked clocks within ANs can be obtained using a time reference from, e.g., GPS, or by communicating a reference time from the central unit of the network to the ANs. However, these methods surely increase the signaling overhead.

C. Channel Model

In order to perform DoA and ToA estimation at LoS-ANs as presented later in Section IV, the following UL single-input-multiple-output (SIMO) multiantenna-multicarrier channel response model for $\mathcal{M}_{\text{AN}}$ antenna elements and $\mathcal{M}_f$ subcarriers is exploited [19]

$$\mathbf{g}_{\ell_k} \approx \mathbf{B}_{\ell_k}(\theta, \varphi, \tau)\boldsymbol{\gamma} + \mathbf{n}, \tag{3}$$

where $\mathbf{g}_{\ell_k} \in \mathbb{C}^{\mathcal{M}_{\text{AN}}\mathcal{M}_f}$ is a channel response vector obtained at the LoS-AN with an index ℓ_k. Furthermore, $\mathbf{B}_{\ell_k}(\theta, \varphi, \tau) \in \mathbb{C}^{\mathcal{M}_{\text{AN}}\mathcal{M}_f \times 2}$ and $\boldsymbol{\gamma} \in \mathbb{C}^2$ denote the polarimetric response of the multiantenna AN ℓ_k and complex path weights, respectively. The model (3) is perturbed with complex-circular zero-mean white-Gaussian noise $\mathbf{n} \in \mathbb{C}^{\mathcal{M}_{\text{AN}}\mathcal{M}_f}$ with variance σ_n^2.

The polarimetric antenna array response is given in terms of the effective aperture distribution function (EADF) [19] such that

$$\begin{aligned}\mathbf{B}_{\ell_k}(\theta, \varphi, \tau) = [&\mathbf{G}_H\mathbf{d}(\varphi, \theta) \otimes \mathbf{G}_f\mathbf{d}(\tau),\\ &\mathbf{G}_V\mathbf{d}(\varphi, \theta) \otimes \mathbf{G}_f\mathbf{d}(\tau)],\end{aligned} \tag{4}$$

where $\otimes$ denotes the Kronecker product, and $\mathbf{G}_H \in \mathbb{C}^{\mathcal{M}_{\text{AN}} \times \mathcal{M}_a\mathcal{M}_e}$ and $\mathbf{G}_V \in \mathbb{C}^{\mathcal{M}_{\text{AN}} \times \mathcal{M}_a\mathcal{M}_e}$ are the EADFs for horizontal and vertical excitations, respectively. Numbers of the determined array response modes, i.e., spatial harmonics, in EADF [19] are denoted as $\mathcal{M}_a$ and $\mathcal{M}_e$ for azimuth and elevation, respectively. Furthermore, $\mathbf{G}_f \in \mathbb{C}^{\mathcal{M}_f \times \mathcal{M}_f}$ is the frequency response of the transceiver, and $\mathbf{d}(\varphi, \theta) \in \mathbb{C}^{\mathcal{M}_a\mathcal{M}_e}$ can be written as

$$\mathbf{d}(\varphi, \theta) = \mathbf{d}(\theta) \otimes \mathbf{d}(\varphi) \tag{5}$$

where $\mathbf{d}(\varphi) \in \mathbb{C}^{\mathcal{M}_a}$ and $\mathbf{d}(\theta) \in \mathbb{C}^{\mathcal{M}_e}$ as well as $\mathbf{d}(\tau) \in \mathbb{C}^{\mathcal{M}_f}$ in (4) are Vandermonde structured vectors. These vectors map the spatial and temporal parameters to the relative frequency domain such that

$$\mathbf{d}(\tau) = \left[e^{-j\pi(\mathcal{M}_f-1)f_0\tau}, \ldots, 1, \ldots, e^{j\pi(\mathcal{M}_f-1)f_0\tau}\right]^{\mathrm{T}}, \tag{6}$$

which can be transformed to correspond the similar $\mathbf{d}(\varphi)$ and $\mathbf{d}(\theta)$ using the relation $\varphi/2 = \pi f_0\tau$, where f_0 denotes the subcarrier spacing of the employed OFDM waveform. The array calibration data, represented using the EADF, can be determined in well-defined propagation environments, e.g., in anechoic chamber [19]. In this paper, the EADFs are assumed to be known for all ANs.

III. Bayesian Filtering Methods

In this paper, two filtering methods for sequential state estimation of non-linear systems, namely EKF and UKF are used and compared. Let us first denote the state of a system at time step k as $\mathbf{s}[k] \in \mathbb{R}^n$. Moreover, an additive and linear state transition model that describes the state evolution between two consecutive time instants $k-1$ and k is assumed such that

$$\mathbf{s}[k] = \mathbf{F}\mathbf{s}[k-1] + \mathbf{u}[k], \tag{7}$$

where $\mathbf{F} \in \mathbb{R}^{n \times n}$ denotes a state transition matrix, and $\mathbf{u}[k] \sim \mathcal{N}(0, \mathbf{Q}_k)$ is a zero-mean Gaussian process noise with covariance $\mathbf{Q}_k \in \mathbb{R}^{n \times n}$. Furthermore, a measurement model that relates the current state $\mathbf{s}[k]$ to the obtained measurements $\mathbf{y}[k] \in \mathbb{R}^m$ through a non-linear function $\mathbf{h} : \mathbb{R}^n \to \mathbb{R}^m$ is expressed as

$$\mathbf{y}[k] = \mathbf{h}(\mathbf{s}[k]) + \mathbf{w}[k], \tag{8}$$

where $\mathbf{w}[k] \sim \mathcal{N}(0, \mathbf{R}_k)$ is a zero-mean Gaussian measurement noise with covariance $\mathbf{R}_k \in \mathbb{R}^{m \times m}$. In addition to the models (7) and (8), also the initial prior distribution of the state $\mathbf{s}[0] \sim \mathcal{N}(\mathbf{m}_0, \mathbf{P}_0)$ is assumed to be known. In the following part of the paper, a general algorithm for the UKF is shortly presented while the algorithm for the well-known EKF can be found, e.g., in [20].

The UKF is an estimation algorithm which uses deterministic sample points, i.e., sigma points to address the limitations of the EKF to some extent with only a slightly increased computational complexity. Instead of approximating the non-linear models, the

generated sigma points are propagated through the involved non-linearities in order to approximate the final posterior distribution [21]. Using this so-called unscented transformation based approximation, high-order information about the desired distribution can be expressed with a relatively small number of fixed points [22]. A compact representation of the UKF in its general form is shown in Algorithm 1, and it follows mainly the same notation as in [20].

The algorithm of the UKF consists of prediction and update phases, in which the non-linearities of the state and measurement models are captured by propagating the deterministic sigma points according to the models. In addition to known initial distribution of $\mathbf{s}[0]$, a scaling parameter λ, which can be expressed in terms of algorithm parameters α and κ, needs to be defined as

$$\lambda = \alpha^2(n + \kappa) - n, \tag{9}$$

where n denotes the dimension of the state, and the parameters α and κ are used to determine the spread of the sigma points around the mean. In literature, the parameter α is usually set to a small positive value, e.g., $1 \leq \alpha \leq 1e^{-5}$, and values of 0 and $3 - n$ are commonly used for the secondary parameter κ [20]–[23].

Generated sigma points are associated with the corresponding weights which can be evaluated such that

$$\begin{aligned} W_m^{(0)} &= \frac{\lambda}{n+\lambda}, & W_m^{(i)} &= \frac{1}{2(n+\lambda)}, \\ W_c^{(0)} &= \frac{\lambda}{n+\lambda} + (1 - \alpha^2 + \beta), & W_c^{(i)} &= \frac{1}{2(n+\lambda)}, \end{aligned} \tag{10}$$

where β is an additional algorithm parameter that can be used to incorporate prior information of the state. For the Gaussian priors, the optimal choice is $\beta = 2$ [23].

IV. UKF-based DoA and ToA Estimation at ANs

In this section, the first phase of the proposed cascaded UKF-based solution depicted in Fig. 2 is shortly described. The proposed method follows the similar EKF-based method proposed and presented more detailed earlier in [14]. In these DoA/ToA UKFs, only a single propagation path with the highest power, which usually corresponds to the LoS path, is tracked. Let us assume the following state for the DoA/ToA UKFs

$$\mathbf{s}[k] = [\tau[k],\, \varphi[k],\, \theta[k],\, \Delta\tau[k],\, \Delta\varphi[k],\, \Delta\theta[k]]^{\mathrm{T}} \in \mathbb{R}^6, \tag{11}$$

where τ, φ, and θ denote ToA, azimuth DoA and elevation DoA, respectively. Furthermore, parameters $\Delta\tau$, $\Delta\varphi$, and $\Delta\theta$ correspond to the rate-of-change of ToA and DoA angles. Considering a linear and nearly constant rate-of-change model, the state transition matrix $\mathbf{F} \in \mathbb{R}^{6\times6}$ and covariance matrix $\mathbf{Q}_k \in \mathbb{R}^{6\times6}$ of the state noise $\mathbf{u}[k] \sim \mathcal{N}(0, \mathbf{Q}_k)$ in (7) can be written as

$$\mathbf{F} = \begin{bmatrix} \mathbf{I}_{3\times3} & \Delta t\mathbf{I}_{3\times3} \\ \mathbf{0}_{3\times3} & \mathbf{I}_{3\times3} \end{bmatrix}, \quad \mathbf{Q}_k = \begin{bmatrix} \frac{\Delta t^3\mathbf{D}}{3} & \frac{\Delta t^2\mathbf{D}}{2} \\ \frac{\Delta t^2\mathbf{D}}{2} & \Delta t\mathbf{D} \end{bmatrix}, \tag{12}$$

respectively. Here, $\mathbf{D} = \mathrm{diag}\,(\sigma_\tau^2, \sigma_\varphi^2, \sigma_\theta^2) \in \mathbb{R}^{3\times3}$ is a diagonal matrix consisting of the variances of the rate-of-change state parameters, and Δt denotes the time difference between the consecutive time steps $k-1$ and k.

Algorithm 1 Unscented Kalman Filter

Initialization Define initial distribution $\mathbf{s}[0] \sim \mathcal{N}(\mathbf{m}_0, \mathbf{P}_0)$
For every iteration $k = 1, \ldots, T$

1) Due to the considered linear state model (7), the *a priori* estimates of the mean and covariance can be obtained as

$$\mathbf{m}_k^- = \mathbf{F}\mathbf{m}_{k-1}, \tag{13}$$
$$\mathbf{P}_k^- = \mathbf{F}\mathbf{P}_{k-1}\mathbf{F}^{\mathrm{T}} + \mathbf{Q}_k. \tag{14}$$

2) Form $2n+1$ sigma points according to

$$\begin{aligned} \mathcal{X}_k^{-(0)} &= \mathbf{m}_k^- \\ \mathcal{X}_k^{-(i)} &= \mathbf{m}_k^- + \sqrt{\lambda+n}\left[\sqrt{\mathbf{P}_k^-}\right]_i \\ \mathcal{X}_k^{-(n+i)} &= \mathbf{m}_k^- - \sqrt{\lambda+n}\left[\sqrt{\mathbf{P}_k^-}\right]_i, \end{aligned} \tag{15}$$

where $i = 1, \ldots, n$.

3) Propagate the sigma points through the measurement model (8)

$$\hat{\mathcal{Y}}_k^{(i)} = \mathbf{h}(\mathcal{X}_k^{-(i)}), \qquad i = 0, 1, \ldots, 2n, \tag{16}$$

4) Compute the measurement mean, measurement covariance and cross-covariance

$$\boldsymbol{\mu}_k = \sum_{i=0}^{2n} W_m^{(i)} \hat{\mathcal{Y}}_k^{(i)}, \tag{17}$$
$$\mathbf{S}_k = \sum_{i=0}^{2n} W_c^{(i)} (\hat{\mathcal{Y}}_k^{(i)} - \boldsymbol{\mu}_k)(\hat{\mathcal{Y}}_k^{(i)} - \boldsymbol{\mu}_k)^{\mathrm{T}} + \mathbf{R}_k, \tag{18}$$
$$\mathbf{C}_k = \sum_{i=0}^{2n} W_c^{(i)} (\mathcal{X}_k^{-(i)} - \mathbf{m}^-)(\hat{\mathcal{Y}}_k^{(i)} - \boldsymbol{\mu}_k)^{\mathrm{T}}. \tag{19}$$

5) Compute the *a posteriori* mean and covariance of $\mathbf{s}[k] \sim \mathcal{N}(\mathbf{m}_k, \mathbf{P}_k)$ using the measurements $\mathbf{y}[k]$

$$\mathbf{K}_k = \mathbf{C}_k\mathbf{S}_k^{-1} \tag{20}$$
$$\mathbf{m}_k = \mathbf{m}_k^- + \mathbf{K}_k(\mathbf{y}[k] - \boldsymbol{\mu}_k) \tag{21}$$
$$\mathbf{P}_k = \mathbf{P}_k^- - \mathbf{K}_k\mathbf{S}_k\mathbf{K}_k^{\mathrm{T}}, \tag{22}$$

End

The actual state parameter estimation is performed in the DoA/ToA UKFs mainly according to the UKF algorithm in Algorithm 1. Since the state parameters φ, θ, and τ are defined on a circle, the generated sigma points are mapped to the feasible regions after carrying out (15) such that $\varphi \in (0, 2\pi]$ and $\theta \in [0, \pi]$. Furthermore, due to the complexity of the estimation problem and complex-valued data, the measurement update phase of the UKF, i.e., the step 5 in Algorithm 1, is performed using a sequential Gauss-Newton method leading to the *a posteriori* mean and covariance estimates such that

$$\mathbf{m}_k = \mathbf{m}_k^- + \mathbf{J}^{-1}\mathbf{r}(\mathbf{m}_k^-), \tag{23}$$
$$\mathbf{P}_k = \mathbf{J}^{-1}. \tag{24}$$

Here, $\mathbf{J}^{-1}$ denotes an approximation of the inverse of the em-

pirical Fisher information matrix (FIM) obtained using weighted statistical linear regression, and $\mathbf{r}$ denotes a cost function gradient evaluated at the *a priori* mean $\mathbf{m}_k^-$. More details regarding such an alternative form of the UKF can be found in [24] whereas the similar EKF-based approach is presented more detailed, e.g., in [14], [25]. Finally, the DoA/ToA UKFs at ANs can be initialized according to the efficient approach proposed for the similar EKF- based method in [14].

V. Joint 3D Positioning and Synchronization

In the second phase of the proposed cascaded solution, the estimated DoAs and ToAs that are communicated to the central entity of a network are, thereafter, fused within the joint positioning and synchronization method as depicted in Fig. 2. In this section, the models used for the 3D positioning and synchronization purposes for both UKF and generalized EKF based DoA/ToA Pos&Clock and DoA/ToA Pos&Sync filters are presented.

In the case of synchronized ANs and assuming the constant velocity (CV) model, which is widely used linear motion model in estimating the position of a moving object, e.g., in [9], the state of the 3D DoA/ToA Pos&Clock UKF and EKF can be written as

$$\mathbf{s}[k] = \left[\mathbf{p}^{\mathrm{T}}[k],\, \mathbf{v}^{\mathrm{T}}[k],\, \rho_{\mathrm{UN}}[k],\, \alpha[k]\right]^{\mathrm{T}} \in \mathbb{R}^8, \tag{25}$$

where $\mathbf{p}[k] = [x[k], y[k], z[k]]^{\mathrm{T}}$ is the 3D position and $\mathbf{v}[k] = [v_x[k], v_y[k], v_z[k]]^{\mathrm{T}}$ is the 3D velocity of a UN. Furthermore, $\rho_{\mathrm{UN}}[k]$ and $\alpha[k]$ denote the clock offset and clock skew of the UN at time step k, respectively. In the scenario where the ANs are phase-locked, the mutual clock offsets of LoS-ANs need to be augmented to the state of the DoA/ToA Pos&Sync UKF and EKF such that $\mathbf{s}[k] \leftarrow \left[\mathbf{s}^{\mathrm{T}}[k],\, \boldsymbol{\rho}_{\ell_{\mathrm{AN}}}^{\mathrm{T}}[k]\right]^{\mathrm{T}} \in \mathbb{R}^{8+L}$, where $\boldsymbol{\rho}_{\ell_{\mathrm{AN}}}[k] = [\rho_{\ell_1}[k], \ldots, \rho_{\ell_L}[k]]^{\mathrm{T}} \in \mathbb{R}^L$ consists of the clock offsets of all L ANs which are in LoS condition with the UN at time step k. Note that all the clock offsets are with respect to a chosen reference AN.

Furthermore, the linear state transition matrix $\mathbf{F} \in \mathbb{R}^{8+L\times 8+L}$ as well as the constant covariance matrix $\mathbf{Q} \in \mathbb{R}^{8+L\times 8+L}$ of the state noise process for the assumed CV model can be written as

$$\mathbf{F} = \mathrm{blkdiag}\left(\begin{bmatrix}\mathbf{I}_{3\times 3} & \Delta t\mathbf{I}_{3\times 3}\\ \mathbf{0}_{3\times 3} & \mathbf{I}_{3\times 3}\end{bmatrix}, \begin{bmatrix}1 & \Delta t\\ 0 & 1\end{bmatrix}, \mathbf{I}_{L\times L}\right), \tag{26}$$

$$\mathbf{Q} = \mathrm{blkdiag}\left(\begin{bmatrix}\frac{\sigma_v^2\Delta t^3\mathbf{I}_{3\times 3}}{3} & \frac{\sigma_v^2\Delta t^2\mathbf{I}_{3\times 3}}{2}\\ \frac{\sigma_v^2\Delta t^2\mathbf{I}_{3\times 3}}{2} & \sigma_v^2\Delta t\mathbf{I}_{3\times 3}\end{bmatrix}, \mathbf{Q}', \mathbf{Q}_\rho\right), \tag{27}$$

where the second and third arguments in $\mathbf{F}$ and $\mathbf{Q}$ correspond to the UN and LoS-ANs clock offset estimations, respectively, such that

$$\mathbf{Q}' = \begin{bmatrix}\frac{\sigma_\eta^2\Delta t^3}{3} & \frac{\sigma_\eta^2\Delta t^2}{2}\\ \frac{\sigma_\eta^2\Delta t^2}{2} & \sigma_\eta^2\Delta t\end{bmatrix}, \qquad \mathbf{Q}_\rho = \sigma_\rho^2\mathbf{I}_{L\times L}, \tag{28}$$

where σ_ρ^2, σ_v^2, and σ_η^2 denote the variances of the LoS-ANs clock offsets, UN velocity and clock skew, respectively.

Moreover, the measurement function $\mathbf{h}_{\ell_i} : \mathbb{R}^{8+L} \rightarrow \mathbb{R}^3$ in (8) that relates the state to the obtained DoA and ToA measurements $\mathbf{y}_{\ell_i}[k] = [\theta_{\ell_i}[k], \varphi_{\ell_i}[k], \tau_{\ell_i}[k]]^{\mathrm{T}}$ estimated at the ℓ_ith AN can be written in the corresponding order as

$$\mathbf{h}_{\ell_i}(\mathbf{s}[k]) = \begin{bmatrix}\arctan\left(\frac{\Delta y_{\ell_i}[k]}{\Delta x_{\ell_i}[k]}\right)\\ \arctan\left(\frac{\Delta z_{\ell_i}[k]}{\|\mathbf{p}[k]-\mathbf{p}_{\ell_i}\|_{2\mathrm{D}}}\right)\\ \frac{\|\mathbf{p}[k]-\mathbf{p}_{\ell_i}\|_{3\mathrm{D}}}{c} + (\rho_{\ell_i}[k] - \rho_{\mathrm{UN}}[k])\end{bmatrix}, \tag{29}$$

where $\Delta x_{\ell_i}[k]$, $\Delta y_{\ell_i}[k]$, $\Delta z_{\ell_i}[k]$ denote the distance between the UN and the ℓ_ith AN in x-, y-, and z-directions, respectively. The Euclidean distances between the UN and the ℓ_ith AN in xy-plane and 3D are denoted as $\|\mathbf{p}[k] - \mathbf{p}_{\ell_i}\|_{2\mathrm{D}}$ and $\|\mathbf{p}[k] - \mathbf{p}_{\ell_i}\|_{3\mathrm{D}}$, and finally c represents the speed of light. Since all the clock offsets are with respect to a pre-defined reference AN, the obtained ToAs contain time offset differences between the UN and received LoS-AN when the transmission is done in a time-stamping manner and, therefore, the difference $(\rho_{\ell_i}[k] - \rho_{\mathrm{UN}}[k])$ needs to be added to the actual propagation delay in (29).

Finally, the measurement model functions and the corresponding measurements as well as the measurement noise terms for all LoS-ANs need to be combined such that $\mathbf{h}(\mathbf{s}[k]) = [\mathbf{h}_{\ell_1}^{\mathrm{T}}(\mathbf{s}[k]), \ldots, \mathbf{h}_{\ell_L}^{\mathrm{T}}(\mathbf{s}[k]))^{\mathrm{T}}$, $\mathbf{y}[k] = [\mathbf{y}_{\ell_1}^{\mathrm{T}}[k], \ldots, \mathbf{y}_{\ell_L}^{\mathrm{T}}[k]]^{\mathrm{T}}$, and $\mathbf{w} \sim \mathcal{N}(0, \mathrm{blkdiag}\left(\mathbf{R}_{k,\ell_1}, \ldots, \mathbf{R}_{k,\ell_L}\right))$. Thereafter, the models (26) and (29) can be used in the proposed DoA/ToA Pos&Clock and Pos&Sync UKFs as such. Moreover, after straightforward differentiation of the measurement function (29), the obtained Jacobian matrix and (26) can be applied to the well-known EKF equations [20] to obtain the proposed 3D DoA/ToA Pos&Clock and Pos&Sync EKFs.

VI. Numerical Evaluations and Analysis

In this section, numerical evaluations are carried out in order to demonstrate and evaluate the performance of the proposed methods in terms of DoA and ToA estimation, positioning, and clock offset estimation accuracy in the outdoor METIS Madrid map environment [26]. For the evaluations, the METIS map-based ray-tracing channel model is implemented using the uniform theory of diffraction (UTD) in order to model the propagation of received beacons [7] as realistically as possible. Furthermore, the transmit power of the tracked UNs is set to $10\,\mathrm{dBm}$, and interfering UNs with the same transmit power are placed on the map randomly $250\,\mathrm{m}$ away from the UN with a density of $1000\,\mathrm{interferers/km^2}$.

The considered 5G network is assumed to deploy OFDMA-based radio access with $240\,\mathrm{kHz}$ subcarrier spacing and $5\,\mathrm{MHz}$ beacon bandwidth, for one UN, comprising of 20 pilot subcarriers [8]. In addition, subframes of length $0.2\,\mathrm{ms}$ containing 14 OFDM symbols are incorporated into the radio frame structure. Furthermore, beacons of the UNs within a specific AN coordination area are assumed to be orthogonal through proper time and frequency multiplexing. Moreover, the proposed filters are updated only every $100\,\mathrm{ms}$ to facilitate communications between the ANs and the central unit of the network as well as relax the UN's energy requirements, while measurements from only $L = 2$ closest LoS-ANs are fused for positioning purposes.

In the evaluations, DoA and ToA estimation as well as positioning and synchronization performance is analysed by averaging over 75 different 3D UN test trajectory realizations. One half of

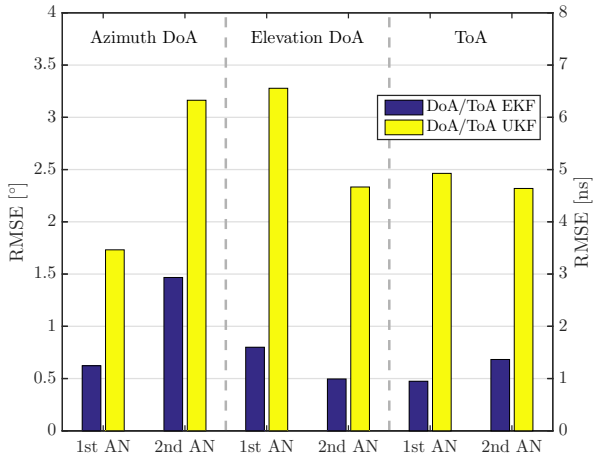

Fig. 3. DoA and ToA estimation results for DoA/ToA UKF-based processing at two closest LoS-ANs in comparison with the EKF-based approach.

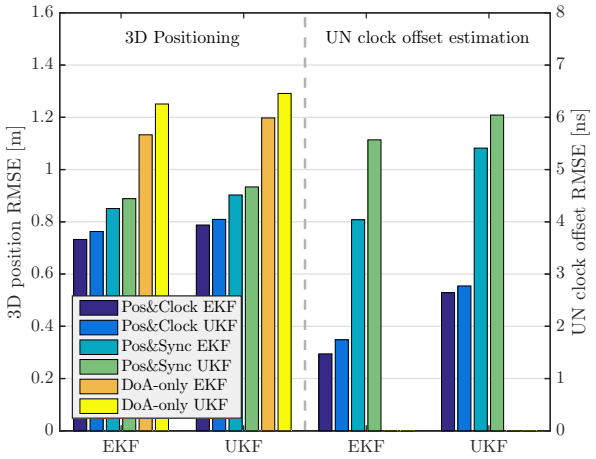

Fig. 4. 3D positioning and UN clock offset estimation RMSEs for all estimation methods and for both DoA/ToA EKF and DoA/ToA UKF scenarios, denoted as EKF and UKF, respectively, after averaging over UN trajectories.

the random trajectories demonstrates a usual vehicle movement in an urban environment with a constant vertical position whereas the other half of the trajectories contains more variation in a vertical direction illustrating applications such as drones. Motion model of the vehicles follows the empirical polynomial model in [27] with a maximum speed of $50\,\mathrm{km/h}$, and the same model is also adopted for drone trajectories containing landings and take-offs as well as short halts on the ground after landing.

A. DoA and ToA Estimation

In order to analyze the estimation accuracy of the proposed DoA/ToA UKF in comparison with the DoA/ToA EKF, root-mean-squared errors (RMSEs) of DoA and ToA tracking for the two closest LoS-ANs are depicted in Fig. 3, after averaging over 75 random UN trajectory realizations on the Madrid grid. Yellow bars in Fig. 3 represent RMSEs for the DoA/ToA UKF whereas blue bars illustrate the performance of the DoA/ToA EKF.

In general, the obtained results are extremely accurate for both methods. However, the DoA/ToA EKF seems to outperform the proposed UKF-based method in both DoA and ToA estimation. Based on the observations, we noticed that the DoA/ToA UKF experienced some disadvantageous divergence with the mapped sigma points and, therefore, the algorithm parameter λ was set to a large value. Although the results are relatively accurate with the DoA/ToA UKF as well, the filter may not fully achieve all of its potential due to the sigma point mapping thus raising a possible topic for the future work. In particular, the sigma-points should exploit the manifold in which the angular parameters are defined. Currently, the conventional form of the UKF and similarly for the sigma-point generation have been employed.

B. Positioning, Clock and Network Synchronization

In the beginning of evaluations, states of the proposed positioning and synchronization methods are initialized. The initial position estimate of the UN is coarsely determined as an average of the known positions of the initial LoS-ANs. Variance of the initial position, denoted as $\sigma^2_{p,0}$ is set to a large value using the distance between the initial UN estimate and LoS-ANs. Furthermore, the initial velocity is set to $\mathbf{v}[0] \sim \mathcal{N}(0, (5\,\mathrm{m/s})^2\mathbf{I}_{3\times3})$ since no additional information in the initialization is used. In the beginning, the clock offset and skew of the UNs are set according to $\rho_{\mathrm{UN}}[0] \sim \mathcal{N}(0, (100\,\mu\mathrm{s})^2)$ and $\alpha[0] \sim \mathcal{N}(25\,\mathrm{ppm}, (30\,\mathrm{ppm})^2)$, respectively, based on [18]. In the phase-locked ANs scenario, the clock offsets of the ANs are initialized similarly to the UNs. In addition, the standard deviation of the clock skew process noise is set to $\sigma_\eta = 6.3 \cdot 10^{-8}$ according to [18] whereas the same value within the filters is increased to $\sigma_\eta = 10^{-4}$ leading to a much better overall performance. Furthermore, the standard deviation of the velocity within the UKF and EKF is set to $\sigma_v = 3.5\,\mathrm{m/s}$. Due to the best overall performance, the algorithm parameters for the both DoA/ToA Pos&Clock and Pos&Sync UKFs are set such that $\alpha = 10^{-3}$, $\beta = 2$, and $\kappa = 0$.

The performance of the proposed DoA/ToA UKF and extended DoA/ToA EKF is evaluated by tracking UNs through random trajectories on the Madrid map. The presented methods in both network synchronization scenarios are carried out using DoA and ToA estimates from both DoA/ToA UKF and DoA/ToA EKF, and finally the results are compared with the 3D DoA-only EKF and UKF. The achieved 3D positioning and UN clock offset estimation RMSE results for each filtering method are illustrated in Fig. 4. Based on the observations, the LoS-ANs clock offset errors are almost identical to the clock offset errors of the UNs and hence these errors are not visualized in this paper. In addition, 2D positioning as well as vertical positioning RMSEs are shown separately in Table I.

Based on the results, the overall positioning performance of the proposed UKF- and EKF-based methods is extremely high. As shown in Fig. 4, the envisioned sub-meter positioning accuracy in 5G [3] can be achieved even in 3D scenarios when accurate ToA measurements are available. As expected, the positioning accuracy of the proposed methods is more accurate in the case of synchronized ANs, i.e., the DoA/ToA Pos&Clock filters, compared to the phase-locked ANs, i.e., the DoA/ToA Pos&Sync filters. In general, a clear relation between the DoA and ToA estimation accuracy, and positioning and synchronization accuracy can also be seen by comparing the results in Fig. 3 and Fig. 4. The overall positioning as well as synchronization results are both better when the DoA/ToA EKF was used due to more accurate DoA

TABLE I. Partitioned 2D and vertical positioning RMSEs for the both DoA/ToA EKF and DoA/ToA UKF measurement estimation scenarios.

	DoA/ToA EKF		DoA/ToA UKF	
	2D (m)	z (m)	2D (m)	z (m)
Pos&Clock EKF	0.71	0.19	0.70	0.32
Pos&Clock UKF	0.73	0.21	0.72	0.33
Pos&Sync EKF	0.83	0.20	0.82	0.34
Pos&Sync UKF	0.86	0.23	0.84	0.35
DoA-only EKF	1.11	0.22	1.12	0.35
DoA-only UKF	1.22	0.27	1.20	0.40

and ToA estimation. Despite the fact that 2D positioning results are better for the DoA/ToA UKF, a clear decrease in vertical positioning can be noticed in Table I. Although the DoA and ToA EKF is slightly outperforming the proposed UKF-based solution, there is only a small difference between the proposed positioning and synchronization methods. Furthermore, the obtained UN clock offset estimates, depicted in Fig. 4, illustrate also the synchronization capability of the proposed methods. In the case of synchronized network, the UN clock offset estimation accuracy is even below $2\,\mathrm{ns}$ at its best. However, the very appealing below $10\,\mathrm{ns}$ clock offset estimates for the UNs as well as LoS-ANs are also achieved with the phase-locked ANs. Based on observations, the EKF tracks the velocity and clock skew of the UN more accurately compared to the UKF after some AN handovers, thus leading to the better overall results. Synchronization accuracy can be occasionally improved by modifying algorithm and filtering parameters within the UKF, while tracking the Doppler would be beneficial for velocity estimation in general.

The behavior of the proposed positioning methods is illustrated in the videos which are available online at `http://www.tut.fi/5G/GLOBECOM16`.

VII. Conclusion

In this paper, UKF- and EKF-based solutions for joint 3D positioning and network synchronization in future 5G UDNs were proposed. First, UKFs are deployed for estimating and tracking the DoAs and ToAs of devices at ANs using UL beacons. Thereafter, a novel UKF solution was proposed to fuse the obtained DoAs and ToAs from LoS-ANs into 3D device position and clock offset estimates while considering realistic clock offsets between devices and ANs as well as mutual clock offsets among the ANs. Furthermore, a similar EKF-based 2D positioning approach was extended for comparison purposes to cover also 3D positioning scenarios. Finally, comprehensive numerical evaluations were carried out considering different 3D motion scenarios for vehicles and UAVs in the realistic Madrid grid environment together with the METIS map-based ray-tracing channel model. Based on the obtained results, below one meter 3D positioning and tracking accuracy can be achieved using the proposed EKF- and UKF-based solutions, while the EKF-based method slightly outperforms the UKF-based method. Simultaneously, the proposed methods also provide extremely accurate nanosecond-scale clock offset estimates for unsynchronized clocks as a valuable by-product.

References

[1] A. Osseiran *et al.*, "Scenarios for 5G mobile and wireless communications: the vision of the METIS project," *IEEE Commun. Mag.*, vol. 52, no. 5, pp. 26–35, May 2014.

[2] F. Boccardi, R. W. Heath, A. Lozano, T. L. Marzetta, and P. Popovski, "Five disruptive technology directions for 5G," *IEEE Commun. Mag.*, vol. 52, no. 2, pp. 74–80, Feb. 2014.

[3] 5G-PPP, "5G empowering vertical industries," Feb. 2015. [Online]. Available: https://5g-ppp.eu/wp-content/uploads/2016/02/BROCHURE_5PPP_BAT2_PL.pdf

[4] NGMN Alliance, "5G white paper," Mar. 2015. [Online]. Available: http://www.ngmn.org/5g-white-paper.html

[5] 5G Forum, "5G white paper: New wave towards future societies in the 2020s," Mar. 2015. [Online]. Available: http://www.5gforum.org/5GWhitePaper/5G_Forum_White_Paper_Service.pdf

[6] A. Dammann, R. Raulefs, and S. Zhang, "On prospects of positioning in 5G," in *Proc. IEEE International Conf. on Communication Workshop (ICCW)*, Jun. 2015, pp. 1207–1213.

[7] METIS, "D1.4 Channel models," Feb. 2015. [Online]. Available: https://www.metis2020.com/wp-content/uploads/METIS_D1.4_v3.pdf

[8] P. Kela, J. Turkka, and M. Costa, "Borderless mobility in 5G outdoor ultra-dense networks," *IEEE Access*, vol. 3, pp. 1462–1476, 2015.

[9] J. Werner, M. Costa, A. Hakkarainen, K. Leppänen, and M. Valkama, "Joint user node positioning and clock offset estimation in 5G ultra-dense networks," in *Proc. IEEE GLOBECOM*, Dec. 2015.

[10] D. Dardari, P. Closas, and P. Djuric, "Indoor tracking: Theory, methods, and technologies," *IEEE Trans. Veh. Technol.*, no. 99, 2015.

[11] R. Di Taranto *et al.*, "Location-aware communications for 5G networks: How location information can improve scalability, latency, and robustness of 5G," *IEEE Signal Process. Mag.*, no. 6, pp. 102–112, Nov. 2014.

[12] V. Aidala, "Kalman filter behavior in bearings-only tracking applications," *IEEE Trans. Aerosp. Electron. Syst.*, vol. AES-15, Jan. 1979.

[13] M. Navarro and M. Najar, "TOA and DOA Estimation for Positioning and Tracking in IR-UWB," in *Proc. IEEE ICUWB*, Sep. 2007.

[14] M. Koivisto *et al.*, "Joint device positioning and clock synchronization in 5G ultra-dense networks," *Submitted to IEEE Trans. Wireless Commun.*, 2016. [Online]. Available: http://arxiv.org/pdf/1604.03322v1.pdf

[15] R. M. Vaghefi and R. M. Buehrer, "Cooperative joint synchronization and localization in wireless sensor networks," *IEEE Trans. Signal Process.*, vol. 63, no. 14, pp. 3615–3627, Jul. 2015.

[16] Z. Irahhauten, H. Nikookar, and M. Klepper, "A joint ToA/DoA technique for 2D/3D UWB localization in indoor multipath environment," in *Proc. IEEE ICC*, Jun. 2012, pp. 4499–4503.

[17] F. Benedetto, G. Giunta, A. Toscano, and L. Vegni, "Dynamic LOS/NLOS statistical discrimination of wireless mobile channels," in *Proc. IEEE VTC Spring*, 2007, pp. 3071–3075.

[18] H. Kim, X. Ma, and B. Hamilton, "Tracking low-precision clocks with time-varying drifts using Kalman filtering," *IEEE/ACM Trans. Netw.*, vol. 20, no. 1, pp. 257–270, Feb. 2012.

[19] A. Richter, "Estimation of radio channel parameters: Models and algorithms," Ph.D. dissertation, Ilmenau University of Technology, http://www.db-thueringen.de/servlets/DerivateServlet/Derivate-7407/ilm1-2005000111.pdf, 2005.

[20] S. Särkkä, *Bayesian filtering and smoothing*. Cambridge University Press, 2013.

[21] S. J. Julier, J. K. Uhlmann, and H. F. Durrant-Whyte, "A new approach for filtering nonlinear systems," in *Proc. American Control Conference*, vol. 3, Jun. 1995, pp. 1628–1632.

[22] S. J. Julier and J. K. Uhlmann, "Unscented filtering and nonlinear estimation," *Proc. IEEE*, no. 3, pp. 401–422, Mar. 2004.

[23] E. A. Wan and R. V. D. Merwe, "The unscented Kalman filter for nonlinear estimation," in *Proc. IEEE Adaptive Systems for Signal Processing, Communications, and Control Symp.*, 2000, pp. 153–158.

[24] R. van der Merwe, "Sigma-point Kalman filters for probabilistic inference in dynamic state-space models," Ph.D. dissertation, Oregon Health & Science University, http://www.cslu.ogi.edu/publications/ps/merwe04.pdf, Apr. 2004.

[25] J. Salmi, A. Richter, and V. Koivunen, "Detection and Tracking of MIMO Propagation Path Parameters Using State-Space Approach," *IEEE Trans. on Signal Process.*, vol. 57, no. 4, pp. 1538–1550, Apr. 2009.

[26] METIS, "D6.1 Simulation guidelines," Oct. 2013. [Online]. Available: https://www.metis2020.com/wp-content/uploads/deliverables/METIS_D6.1_v1.pdf

[27] R. Akcelik and D. C. Biggs, "Acceleration profile models for vehicles in road traffic," *Transportation Science*, no. 1, pp. 36–54, Feb. 1987.